
Explicit Critic Guidance for Aligning Diffusion Models

Zhengyang Liang
University of Toronto
Vector Institute

Qihang Zhang
The Chinese University of Hong Kong

Ceyuan Yang
The Chinese University of Hong Kong

Abstract

Online reinforcement learning is becoming increasingly important for aligning diffusion models with non-differentiable objectives. However, existing methods still face limitations in assigning fine-grained credit along denoising trajectories and in realizing stable value-based optimization. We propose a state-aligned latent actor-critic framework for diffusion post-training, in which the diffusion model serves as its own timestep-conditioned value function and predicts values directly on noisy latent states. This enables trajectory-level PPO training, supports stable actor-critic optimization with simple conditioning and value pretraining strategies, and naturally allows the learned critic to be reused for inference-time steering. We further extend the framework to multi-reward optimization, where joint training with complementary rewards helps alleviate reward hacking. Across both UNet- and DiT-based backbones, our method consistently outperforms prior group-relative RL and actor-critic baselines on single-reward and multi-reward benchmarks, while test-time steering provides additional gains in generation quality.

1 Introduction

Post-training is becoming an increasingly important stage for visual generative models. Although large-scale pretraining [11, 61, 74, 37, 84] already yields strong visual quality, pretrained models often remain suboptimal on properties that users directly care about, including prompt faithfulness, compositional correctness [17, 24], text rendering [6], aesthetics, and human preference [77, 47, 79, 27, 72]. Reinforcement learning [60, 1, 35, 63, 92, 58, 23, 51, 70, 2] is particularly appealing in this setting because it enables optimization with respect to verifiable and task-specific objectives, including learned preference models and rule-based rewards.

A central challenge in diffusion post-training is *credit assignment*. Diffusion models [22, 68, 69, 8, 40, 45] generate samples through multi-step denoising trajectories, whereas rewards are typically defined only on the final decoded image. The problem is therefore not only to maximize terminal reward, but to assign it to the intermediate noisy states and denoising decisions that produced it. Group-relative methods [43, 81, 7] partially avoid this issue by comparing samples within a group, but the resulting signal remains coarse and trajectory-level. Explicit actor-critic methods are in principle better suited to this setting, yet existing diffusion critics [91, 48] are typically defined in pixel space: they evaluate reconstructed clean-image proxies rather than the actual noisy latent states visited by the policy. This mismatch weakens alignment between critic and policy, makes value estimation brittle for structured or discrete rewards, and incurs substantial decoding overhead. Moreover, explicit actor-critic training is often unstable, as poorly conditioned value estimates can quickly undermine policy optimization.

To address these issues, we propose a *state-aligned latent actor-critic* framework in which the diffusion model itself serves as a timestep-conditioned value network and predicts $V_\phi(z_t, t, y)$ directly



Figure 1: **Text-conditioned image generation results from our SD3.5M models.** All samples are generated **without** classifier free guidance.

on noisy latent states. This requires only lightweight modifications to the pretrained diffusion backbone, allowing the critic to inherit the model’s generative prior while operating on the same state space and diffusion-native features as the policy. The resulting critic is naturally noise-aware, avoids repeated image decoding, and can be reused at inference time, where its latent-space gradients provide a direct steering signal during sampling. To make this formulation practical, we further identify timestep-aware conditioning and a short value pretraining stage as simple but effective techniques for improving training stability and efficiency. As illustrated in Fig. 1, the framework also enables *CFG-free* post-training, reducing memory overhead and training cost while avoiding the color saturation artifacts and instability often introduced by classifier-free guidance.

A stronger optimizer, however, also makes reward misspecification more visible. In diffusion post-training, reward hacking often appears as shortcut solutions that improve the target metric while degrading unmeasured aspects of image quality. For example, optimizing a compositional reward in isolation may improve the target score while sacrificing background diversity or aesthetics, whereas complementary rewards can counteract such collapse modes. This motivates our multi-reward extension: we equip the shared latent backbone with separate value heads so that multiple rewards can regularize one another while still benefiting from a common timestep-aware representation. In this way, multi-reward optimization provides a practical mechanism for mitigating proxy overoptimization in diffusion RL.

In summary, our contributions are as follows:

- We propose a state-aligned latent critic framework for diffusion post-training, which converts a pretrained diffusion model into its own value network with lightweight modifications and supports both latent-state value prediction and inference-time steering.
- We identify timestep-aware conditioning and value pretraining as simple but effective techniques for stabilizing and accelerating explicit actor-critic diffusion training.
- We extend the framework to multi-reward optimization, where joint training with complementary rewards helps mitigate proxy overoptimization and alleviate reward hacking.
- Across both single-reward and multi-reward benchmarks, our method consistently outperforms prior group-relative RL and actor-critic baselines, with additional gains from inference-time steering.

2 Related Work

Diffusion alignment. Recent work on aligning diffusion models can be broadly grouped into reward-based fine-tuning, preference optimization, and online reinforcement learning. Early approaches align text-to-image models with human or learned feedback by collecting preference data, training

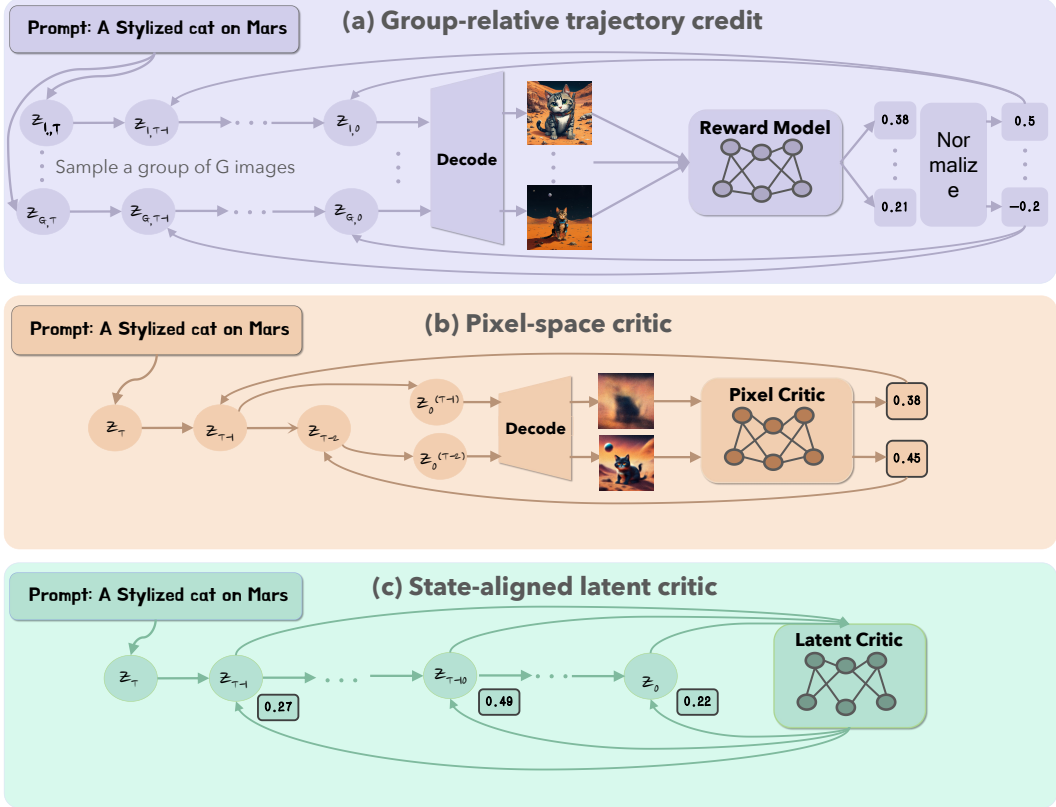


Figure 2: **Illustration of three credit assignment strategies in diffusion RL.** GRPO-style methods assign one relative signal to each trajectory by groupwise reward comparison. Pixel-space critics score reconstructed images decoded from intermediate latents, leading to proxy-state evaluation. Our method instead learns a critic directly on noisy latent states, enabling state-dependent and state-aligned credit assignment as well as inference-time steering from the same learned critic.

reward models, and fine-tuning the generator with reward-based objectives [30, 12, 53, 80]. For differentiable rewards, alignment can also be performed by backpropagating reward gradients through the denoising process [79, 5, 54, 55]. Another line of work adapts preference optimization methods to diffusion models, including DPO-style formulations [57, 78, 44, 36, 33, 88, 87, 15, 82]. More recently, online RL methods [4, 14, 60, 20, 49, 91, 48, 90] optimize diffusion models directly against downstream rewards. This line has also been extended to Group-Relative style policy gradient method [43, 81, 34, 32], which bypass the training of critic. Compared with these methods, our work focuses on value-based post-training with an explicit critic learned on the same noisy latent trajectory as the policy. We provide extended discussion in Appendix D.

3 Method

3.1 Problem setup

We briefly define the sequential decision-making view of diffusion post-training used throughout the paper. Let z_t denote the noisy latent at timestep t , and let y be the text condition. A latent diffusion or flow-based generator produces an image by iteratively updating z_t along a denoising trajectory from noise to data. We view this process as a finite-horizon sequential decision problem. At step k , the state is

$$s_k = (z_{t_k}, t_k, y),$$

and the action a_k is the model prediction used by the sampler, e.g., a noise, score, or velocity prediction depending on the backbone. The transition is induced by the sampler. After the final step, the denoised latent is decoded and evaluated by a reward function, yielding a terminal reward

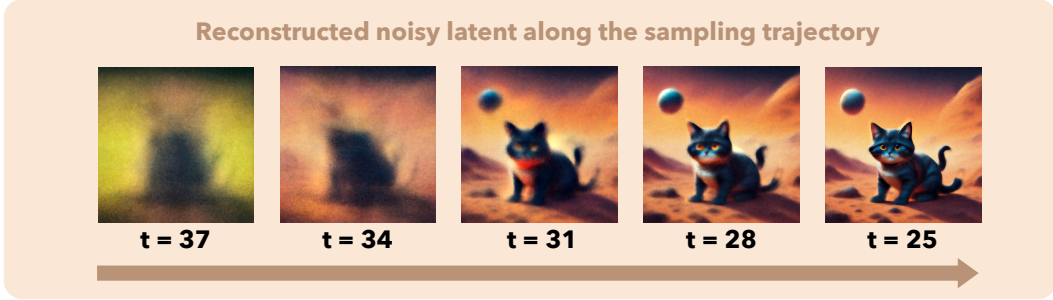


Figure 3: **Reconstructed noisy latent along the sampling chain.** We visualize selected intermediate latent states by reconstructing them into image space. Although early reconstructions are blurry and out of distribution for pixel-space evaluators, the underlying noisy latents remain on the diffusion denoising trajectory, motivating a critic that operates directly in latent space.

$r_T = r(x, y)$, with $r_k = 0$ for $k < T$. The objective is to maximize the expected terminal reward over the denoising trajectory. To obtain intermediate feedback, we learn a timestep-conditioned value function

$$V_\phi(s_t, t) \approx \mathbb{E}_\pi[R | s_t], \quad (1)$$

which estimates the expected terminal return from an intermediate noisy latent state. The critic is then used to compute advantages for PPO-style policy updates. We optimize the actor and critic network following [60].

3.2 Learning a State-Aligned Critic in Latent Space

Credit assignment. As discussed in Sec. 1, existing work either bypasses explicit critic or learning diffusion critics operate on proxy states rather than the actual noisy latents visited by the policy. We address this by learning a critic directly on the denoising trajectory. We provide an illustration of three mechanisms in Fig. 2. Moreover, as we show in Fig. 3, such reconstructed images are often out of distribution for pixel-space evaluators such as CLIP [56] or BLIP [31], whereas the corresponding noisy latents remain in distribution for the diffusion model itself. Pixel critic requires extra finetuning to adapt to these inputs. These observations motivate our central design choice: effective diffusion RL requires a critic that assigns value directly on the noisy latent trajectory.

State-aligned Latent Critic Based on this view, we learn a timestep-conditioned latent critic

$$V_\phi(z_t, t, y),$$

directly on the denoising trajectory. Unlike pixel-space critics, our critic stays entirely in latent space, shares the same trajectory representation as the policy, and remains naturally aware of timestep and noise level. We initialize the critic from the actor, which is a pretrained diffusion model, and convert it into a scalar value predictor with lightweight architectural modifications. The overview for our architecture design is shown in Fig. 4.

UNet critic. For a UNet backbone, we first process the noisy latent with the standard denoising network, then patchify the resulting feature map into tokens. A learnable summary token is appended and passed through a lightweight attention head, followed by a small MLP that predicts the scalar value $V_\phi(z_t, t, y)$.

DiT critic. For a diffusion transformer [52], inspired by previous work [39], we insert lightweight critic branches at a few intermediate (layer 7, 15, 23) layers. Each branch uses a learnable query token to aggregate information from image tokens, producing a critic token for that layer. The critic tokens from selected layers are concatenated and mapped to a scalar value through an MLP head.

Stabilizing Critic Training. Directly training the latent critic is often unstable and inefficient. In practice, the critic is initialized from a pretrained diffusion backbone whose original output is a tensor-valued denoising prediction rather than a scalar return, which leads to poorly scaled value estimates and noisy policy updates. To improve critic learning, we adopt two simple techniques: (1) **Timestep conditioning on the value head.** Although the shared backbone already receives t as input, we find it beneficial to additionally condition the final value head on the timestep via

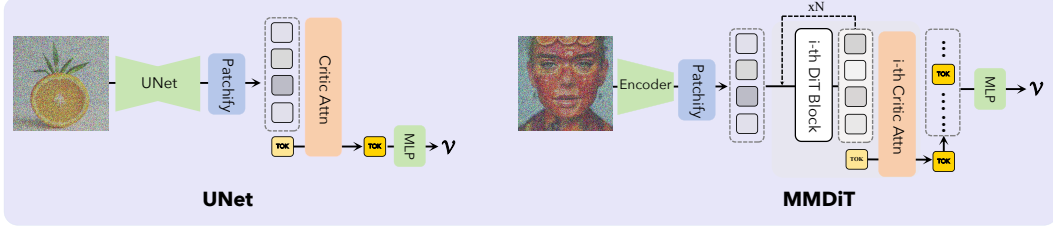


Figure 4: **Architecture overview over UNet and Diffusion Transformer.** We initialize the value network with pretrained diffusion models. Attention layer and MLP are added to predict critic scalar.

AdaLN-style modulation. This gives the head direct access to the noise level, which improves value prediction across the denoising trajectory. (2) **Value pretraining.** Before joint actor-critic optimization, we run a short warm-up stage in which trajectories are sampled from the current policy but only the critic is updated. Concretely, given an intermediate state $s_k = (z_{t_k}, t_k, y)$ and its Monte Carlo return target \hat{R}_k , we optimize the critic with a regression loss

$$\mathcal{L}_{\text{value}}(\phi) = \mathbb{E}_{(s_k, \hat{R}_k)} \left[(V_\phi(s_k) - \hat{R}_k)^2 \right]. \quad (2)$$

This warm-up yields better value estimates and improves the stability and efficiency of subsequent PPO training.

Inference-time steering. Because our critic is defined on the same noisy latent states as the policy, it can be directly reused at inference time as a guidance module [21, 8]. Intuitively, the gradient $\nabla_{z_t} V_\phi$ points toward latent regions where the critic predicts higher terminal reward, playing a role analogous to classifier guidance but with reward replacing class likelihood. We compute the steering direction as:

$$g_t = \nabla_{z_t} V_\phi(z_t, t, y). \quad (3)$$

We then inject this direction into the sampler update. For a DDIM [67]-style sampler with noise prediction $\epsilon_\theta(z_t, t, y)$, we modify the predicted noise as

$$\hat{\epsilon}_\theta(z_t, t, y) = \epsilon_\theta(z_t, t, y) - \eta \sqrt{1 - \bar{\alpha}_t} g_t, \quad (4)$$

where η controls the steering strength and the factor $\sqrt{1 - \bar{\alpha}_t}$ matches the perturbation magnitude to the noise level at timestep t . For flow-matching / rectified-flow [45, 40] samplers with velocity prediction $v_\theta(z_t, t, y)$, we add the critic direction directly to the predicted velocity:

$$\hat{v}_\theta(z_t, t, y) = v_\theta(z_t, t, y) + \eta g_t. \quad (5)$$

In both cases, the critic-derived direction biases the denoising trajectory toward regions the critic predicts as higher-value, effectively turning the PPO-trained critic into an inference-time guidance module.

3.3 Multi-Reward Optimization to mitigate reward hacking

Reward hacking. We observe a consistent form of reward hacking during diffusion post-training: the model improves the target reward by exploiting shortcut patterns that degrade unmeasured aspects of image quality. For human-preference rewards, hacking often manifests as collapsing to recurring styles, colors, or visual templates favored by the reward model; for verifiable rewards, it is typically more severe, e.g., missing or simplified backgrounds and repetitive reward-favored structures (Fig. 5 (top)). A common mitigation is KL regularization toward the base model, which indeed slows reward growth by pulling the policy back toward the pretrained distribution. However, we find that KL primarily changes the optimization timescale: when KL-regularized and non-regularized runs reach comparable reward values, they exhibit qualitatively similar hacking behavior, indicating that KL alone does not resolve reward misspecification.

Multi-reward optimization. Reward hacking is especially pronounced when optimizing verifiable rewards, and can emerge very early in training. As illustrated in Fig. 5, when our model is trained with GenEval alone, it often converges to shortcut solutions with simplified composition and missing background content, even when the target objects are correctly generated. Extending our framework

to a multi-reward setting provides an effective counterbalance: by jointly optimizing GenEval with an auxiliary human-preference reward such as HPS, the model retains the desired objects while producing richer scenes, better aesthetics, and more natural compositions. In this sense, multi-reward training reduces the severity of reward hacking and delays its onset, although it does not eliminate the problem entirely; with sufficiently long training, shortcut behaviors can still dominate, so early stopping remains an important practical safeguard.

Motivated by these observations, we optimize the policy against a set of reward functions $\{r^{(m)}\}_{m=1}^M$ using a shared latent backbone together with one lightweight value head per reward. A naive shared-head design consistently yields slow PPO progress, since different rewards have different scales and emphasize different visual attributes. Instead, each head predicts its own value $V_{\phi}^{(m)}(z_t, t, y)$ from the same timestep-aware latent features, while learning reward-specific scale and bias. This design amortizes the expensive diffusion feature extraction across objectives, reduces interference between heterogeneous rewards, and enables stable joint optimization in the multi-reward regime.



Figure 5: **Qualitative comparison of single-reward and multi-reward optimization.** GenEval-only training (top) often produces shortcut solutions with simplified composition and missing background content. Adding HPS (bottom) preserves the target objects while improving overall visual quality.

4 Experiments

We evaluate our post-training method on a diverse set of image generation tasks and compare it with recent diffusion RL baselines, including DDPO and GRPO, with a focus on single-reward optimization efficiency. We then move to the multi-reward setting to test whether our shared backbone and per-reward heads can handle heterogeneous scales and signals. In addition, we present the results of our inference-time critic guidance, showing that the same critic used for PPO can be reused at sampling time to further improve the generated images without training. All experiments are run on two backbone families: (1) a UNet-based latent diffusion model, **SD 1.5**, and (2) a diffusion-transformer model, **SD 3.5 M**, to verify that our design works for both convolutional and DiT-style architectures. Finally, we provide extensive ablations on our proposed designs.

Implementation. All models are trained for 300 iterations. For DDPO [4] and GRPO [43, 81] we follow the training hyperparameters in DanceGRPO [81]. GRPO requires sampling multiple images for the same prompt to form a group and compute relative advantages, while DDPO and our PPO-based method sample only one image per prompt. To keep the comparison fair, we increase the number of distinct prompts in each iteration for DDPO and for our method so that the total number of generated images per iteration matches that of GRPO. Besides, we find online RL can work without classifier-free guidance [22]. Therefore, we disable cfg for all experiments.

Table 1: **Single-reward optimization** on SD1.5 and SD3.5-M under different reward types. Our method achieves the best results across both diffusion models and reward types. DDPO fails with SD3.5M on GenEval and OCR.

Model	Method	CLIP \uparrow	HPSv2.1 \uparrow	PickScore \uparrow	GenEval \uparrow	OCR \uparrow
SD1.5	Base	0.2250	0.1727	-1.0929	0.1558	0.066
	DDPO	0.3233	0.2752	0.2187	0.5455	0.2351
	GRPO	0.3342	0.3779	0.2406	0.5888	0.2518
	Ours	0.3431	0.3912	0.2458	0.6392	0.2648
SD3.5-M	Base	0.2275	0.1750	-1.4298	0.2013	0.0002
	DDPO	0.2822	0.2246	0.1976	div	div
	GRPO	0.3006	0.3604	0.2304	0.9620	0.5653
	Ours	0.3029	0.3642	0.2320	0.9758	0.5876

Table 2: **Multi-reward optimization** on SD1.5 and SD3.5-M. Our approach is the most efficient among all methods. On GenEval, our method outperforms GRPO by a large margin while remaining comparable on CLIP and HPSv2.1.

Model	Method	CLIP \uparrow	HPSv2.1 \uparrow	GenEval \uparrow	Sum \uparrow
SD1.5	Base	0.2250	0.1727	0.1558	0.5535
	DDPO	0.2590	0.2995	0.3830	0.9415
	GRPO	0.2811	0.3474	0.4688	1.0973
	Ours	0.2896	0.3441	0.4986	1.1323
SD3.5-M	Base	0.2275	0.1750	0.2013	0.6038
	DDPO	div	div	div	div
	GRPO	0.2803	0.3392	0.7705	1.3927
	Ours	0.2772	0.3130	0.9241	1.5143

4.1 Single-Reward Benchmarks

We first evaluate our method in the single-reward setting, where the goal is to make the model improve as fast as possible under one target reward. We group the reward models into three categories. (i) **Text-image alignment**: We use CLIP to measure how well the generated image matches the text prompt. (ii) **Human-preference rewards**: we use HPSv2.1 and PickScore, both trained on human preference data, to assign higher scores to images that are better aligned with human judgments. (iii) **Verifiable rewards**: we use GenEval, which checks whether the compositional constraints in the prompt are satisfied, and an OCR-based text-rendering reward, which verifies whether the rendered text in the image matches the prompt.

We provide the results in Table 1. Overall, PPO wins on almost all metrics for both backbones, with especially clear gains on verifiable rewards such as GenEval and OCR, suggesting that per-timestep value estimates are particularly beneficial when the reward signal is sparse and discrete. We also observe that DDPO can fail to train in some of the large-scale settings, while both GRPO and our method remain stable. GRPO needs multi-sample groups per prompt to estimate advantages, but our method, like DDPO, uses only one sample per prompt; the difference between our method and DDPO is that our advantages come from the critic trained in Sec. 3, showing that the critic can supply sufficiently accurate value estimates. Qualitative comparison in Fig. 6 shows that our method achieves better visual appearance and precise control.

4.2 Multi-Reward Joint Optimization

We next evaluate whether our method remains effective when multiple heterogeneous rewards must be optimized at the same time. From the three categories we pick one representative reward each: CLIP for text-image alignment, HPSv2.1 for human-preference signals, and GenEval for non-differentiable compositional constraints. We train with equal weights 1:1:1 on these three rewards. In every iteration we also sample prompts and the corresponding metadata from the three datasets with a fixed ratio 1:1:1, so that each update sees a balanced mix of alignment, preference, and discrete objectives.

The results are shown in Table 2. As shown in the table, when optimizing multiple rewards simultaneously, all methods improve more slowly on any single metric, which is expected be-



Figure 6: **Qualitative comparison between our model and baselines.**

Table 3: Comparison between our proposed critic and previous pixel critics.

(a) Ablation on critic design (HPSv2.1 reward).

Critic	CLIP	BLIP	HPSv2.1	Ours
Results \uparrow	0.3323	0.3612	0.3495	0.3912

(b) Efficiency comparison between different critics.

Critic	Ours	CLIP [56]	BLIP [31]	HPSv2.1 [77]
Value Computing	10s	33s	35s	28s
Training	20s	78s	86s	52s

cause the three signals can be partially conflicting. DDPO does not converge well on SD3.5-M in this mixed setting. Both GRPO and our method make stable progress on all three rewards; however, on GenEval our method is noticeably stronger than GRPO, while on CLIP and HPSv2.1 we stay close to or slightly better than GRPO. This indicates that the learned critic can capture the advantages coming from different reward sources and provide a cleaner training signal, making it more effective in the multi-reward regime.

4.3 Inference-Time Steering

We further test whether the critic trained together with PPO can be used purely at inference time to steer sampling and improve rewards, without any extra finetuning. Starting from the post-trained models (SD1.5 and SD3.5-M), we compare four inference-time strategies under the same sampling budget per prompt:

- (1) **Best-of- n (BoN)**: draw n i.i.d. samples and keep the highest-reward one.
- (2) **SMC**: following FK-steering [75, 89, 66], maintain n particles, evaluate the reward at intermediate timesteps by pushing samples to x_0 , and resample according to normalized rewards.
- (3) **Our Critic Gradient Guidance**: add the critic-derived direction at every denoising step, generating only one sample per prompt.
- (4) **Critic Gradient Guidance + BoN**: run critic-guided sampling to generate n candidates, then apply BoN selection.

We evaluate on HPSv2.1 (additional rewards are reported in Appendix D). The results are shown in Fig. 7. On SD1.5, critic guidance alone already surpasses BoN. On SD3.5-M it falls below BoN but still clearly improves over the post-trained baseline and SMC. Combining critic guidance with BoN yields the best performance on both backbones, indicating that trajectory steering and reward-based selection are complementary. Notably, critic guidance generates only a single sample per prompt, whereas BoN and SMC require n forward passes—yet it matches or exceeds BoN on SD1.5 despite this $n \times$ computational advantage.

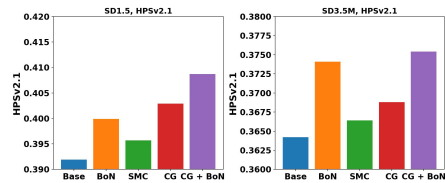


Figure 7: Inference-time steering on HPSv2.1 for post-trained SD1.5 / SD3.5-M. We compare BoN, SMC, our critic gradient guidance, and guidance + BoN. Base refers to the RL post-trained model.

4.4 Ablation Studies

We conduct a series of ablations to demonstrate the effectiveness of our designs proposed in Sec.3.

4.4.1 Critic Architecture Choices

We first compare our diffusion model critic with several commonly used reward/vlm repurposed as a critic. All ablations are run on the HPSv2.1 reward to keep the setting consistent. We test: (i) CLIP, (ii) BLIP (iii) HPSv2.1 reward model. We then compare them to our proposed critic design.

From Table 3, our latent critic achieves the highest final reward on HPSv2.1, outperforming CLIP, BLIP, and using the reward model itself as a critic. Table 3b further shows that pixel-space critics are substantially more expensive: our value computation takes 10s, compared with 28–35s for HPSv2.1/CLIP/BLIP (i.e., $2.8 \times$ – $3.5 \times$ slower), and our training step takes 20s, compared with 52–86s for HPSv2.1/CLIP/BLIP (i.e., $2.6 \times$ – $4.3 \times$ slower). Overall, operating directly in latent space with a timestep-conditioned critic yields both higher rewards and markedly better efficiency.

Table 4: **Ablation on value pretraining.** Value pretraining improves performance, especially on verifiable rewards.

	vp 15it	vp 50it	vp 100it	w/o vp
GenEval \uparrow	0.6392	0.6138	0.5932	0.5419

Table 5: **Ablation on separate value heads.** Separate heads consistently outperform a shared head across all rewards.

	CLIP \uparrow	HPSv2.1 \uparrow	GenEval \uparrow
Separate head	0.2896	0.3441	0.4986
Shared head	0.2804	0.3138	0.4238

4.4.2 Effect of Value Pretraining

Next, we evaluate the effect of the value-pretraining phase. We run this ablation on GenEval, which gives a sparser and less smooth signal than HPSv2.1. We compare two training settings: (i) training PPO directly from the diffusion-initialized critic without value pretraining, and (ii) doing a short value-pretraining stage before enabling actor updates. We keep all other hyperparameters the same. As shown in Table 4, adding value pretraining improves the final performance. This supports our claim that warming up the critic gives the policy better advantage estimates, especially for hard or discrete rewards.

4.4.3 Separate Heads for Multi-reward Training

We study the critic design for the multi-reward setting, where we share the diffusion backbone but predict each reward with a separate lightweight MLP value head. We compare this design to a shared-head variant that regresses all rewards with a single scalar head. As shown in Table 5, separate heads consistently outperform the shared head across all rewards (CLIP, HPSv2.1, and GenEval), suggesting that decoupling value prediction reduces interference between heterogeneous objectives and better accommodates reward-specific scales and semantics.

4.4.4 Effect of CFG on training.

We ablate the effect of classifier-free guidance (CFG) on training and use *CFG-free* training ($cfg = 1.0$) in all main experiments. Besides reducing memory usage and improving training speed, CFG-free training also yields the best optimization behavior. As shown in Fig. 8, larger CFG scales improve the initial reward, but lead to slower subsequent gains and more unstable reward curves. In particular, higher CFG introduces stronger fluctuations, and $cfg = 10.0$ even shows reward degradation at later training stages. In contrast, $cfg = 1.0$ achieves both the most stable trajectory and the highest final reward.

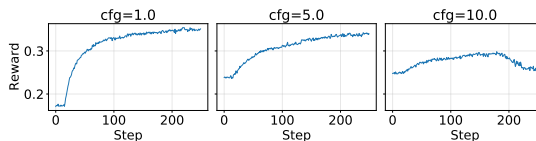


Figure 8: **Effect of CFG on training.** Higher CFG improves the initial reward, but leads to slower and less stable optimization. CFG-free ($cfg = 1.0$) achieves the best final reward.

4.4.5 MLP conditioning

Table 6 ablates conditioning for the critic MLP head. We find that timestep conditioning is essential: it improves HPSv2.1 from 0.3496 to 0.3642 without text conditioning, and from 0.3524 to 0.3630 with text conditioning. In contrast, text conditioning only provides a small gain when time conditioning is absent, and does not help once timestep conditioning is already included. We therefore use timestep conditioning for the critic head and omit additional text conditioning.

Table 6: **Ablation on critic-head conditioning.**

Time cond.	Text cond.	HPSv2.1 \uparrow
\times	\times	0.3496
\times	\checkmark	0.3524
\checkmark	\times	0.3642
\checkmark	\checkmark	0.3630

5 Conclusion

We present a stable, efficient, and scalable actor-critic framework for post-training diffusion models. Our method makes three contributions: (1) converting diffusion backbones into timestep-aware critics

with value pretraining enables stable and sample-efficient PPO training; (2) a lightweight multi-value-head design supports multi-reward optimization; and (3) the learned critic can be reused for inference-time steering, providing performance gains beyond training. These components establish a practical recipe for applying reinforcement learning to modern diffusion models.

References

- [1] Arash Ahmadian, Chris Cremer, Matthias Gallé, Marzieh Fadaee, Julia Kreutzer, Olivier Pietquin, Ahmet Üstün, and Sara Hooker. Back to basics: Revisiting reinforce style optimization for learning from human feedback in llms. *arXiv preprint arXiv:2402.14740*, 2024.
- [2] Yuntao Bai, Andy Jones, Kamal Ndousse, Amanda Askell, Anna Chen, Nova DasSarma, Dawn Drain, Stanislav Fort, Deep Ganguli, Tom Henighan, et al. Training a helpful and harmless assistant with reinforcement learning from human feedback. *arXiv preprint arXiv:2204.05862*, 2022.
- [3] Yuntao Bai, Saurav Kadavath, Sandipan Kundu, Amanda Askell, Jackson Kernion, Andy Jones, Anna Chen, Anna Goldie, Azalia Mirhoseini, Cameron McKinnon, Carol Chen, Catherine Olsson, Christopher Olah, Danny Hernandez, Dawn Drain, Deep Ganguli, Dustin Li, Eli Tran-Johnson, Ethan Perez, Jamie Kerr, Jared Mueller, Jeffrey Ladish, Joshua Landau, Kamal Ndousse, Kamile Lukosuite, Liane Lovitt, Michael Sellitto, Nelson Elhage, Nicholas Schiefer, Noemi Mercado, Nova DasSarma, Robert Lasenby, Robin Larson, Sam Ringer, Scott Johnston, Shauna Kravec, Sheer El Showk, Stanislav Fort, Tamera Lanham, Timothy Telleen-Lawton, Tom Conerly, Tom Henighan, Tristan Hume, Samuel R. Bowman, Zac Hatfield-Dodds, Ben Mann, Dario Amodei, Nicholas Joseph, Sam McCandlish, Tom Brown, and Jared Kaplan. Constitutional ai: Harmlessness from ai feedback, 2022. URL <https://arxiv.org/abs/2212.08073>.
- [4] Kevin Black, Michael Janner, Yilun Du, Ilya Kostrikov, and Sergey Levine. Training diffusion models with reinforcement learning. In *The Twelfth International Conference on Learning Representations*, 2024. URL <https://openreview.net/forum?id=YCWjhGrJFD>.
- [5] Kevin Clark, Paul Vicol, Kevin Swersky, and David J. Fleet. Directly fine-tuning diffusion models on differentiable rewards. In *The Twelfth International Conference on Learning Representations*, 2024. URL <https://openreview.net/forum?id=1vmSEVL19f>.
- [6] Cheng Cui, Ting Sun, Manhui Lin, Tingquan Gao, Yubo Zhang, Jiaxuan Liu, Xueqing Wang, Zelun Zhang, Changda Zhou, Hongen Liu, Yue Zhang, Wenyu Lv, Kui Huang, Yichao Zhang, Jing Zhang, Jun Zhang, Yi Liu, Dianhai Yu, and Yanjun Ma. Paddleocr 3.0 technical report, 2025. URL <https://arxiv.org/abs/2507.05595>.
- [7] Haoyou Deng, Keyu Yan, Chaojie Mao, Xiang Wang, Yu Liu, Changxin Gao, and Nong Sang. Densegrp: From sparse to dense reward for flow matching model alignment. *arXiv preprint arXiv:2601.20218*, 2026.
- [8] Prafulla Dhariwal and Alexander Nichol. Diffusion models beat gans on image synthesis. *Advances in neural information processing systems*, 34:8780–8794, 2021.
- [9] Zheng Ding and Weirui Ye. TreeGRPO: Tree-advantage GRPO for online RL post-training of diffusion models. In *The Fourteenth International Conference on Learning Representations*, 2026. URL <https://openreview.net/forum?id=3rZdp4TmUb>.
- [10] Arnaud Doucet et al. *Sequential Monte Carlo methods in practice*, volume 1. Springer.
- [11] Patrick Esser, Sumith Kulal, Andreas Blattmann, Rahim Entezari, Jonas Müller, Harry Saini, Yam Levi, Dominik Lorenz, Axel Sauer, Frederic Boesel, et al. Scaling rectified flow transformers for high-resolution image synthesis. In *Forty-first international conference on machine learning*, 2024.
- [12] Jiajun Fan, Shuaike Shen, Chaoran Cheng, Yuxin Chen, Chumeng Liang, and Ge Liu. Online reward-weighted fine-tuning of flow matching with wasserstein regularization. In *The Thirteenth International Conference on Learning Representations*, 2025.

- [13] Tiantian Fan, Lingjun Liu, Yu Yue, Jiaze Chen, Chengyi Wang, Qiying Yu, Chi Zhang, Zhiqi Lin, Ruofei Zhu, Yufeng Yuan, Xiaochen Zuo, Bole Ma, Mofan Zhang, Gaohong Liu, Ru Zhang, Haotian Zhou, Cong Xie, Ruidong Zhu, Zhi Zhang, Xin Liu, Mingxuan Wang, Lin Yan, and Yonghui Wu. Truncated proximal policy optimization, 2025. URL <https://arxiv.org/abs/2506.15050>.
- [14] Ying Fan, Olivia Watkins, Yuqing Du, Hao Liu, Moonkyung Ryu, Craig Boutilier, Pieter Abbeel, Mohammad Ghavamzadeh, Kangwook Lee, and Kimin Lee. Dpok: Reinforcement learning for fine-tuning text-to-image diffusion models. *Advances in Neural Information Processing Systems*, 36:79858–79885, 2023.
- [15] Hiroki Furuta, Heiga Zen, Dale Schuurmans, Aleksandra Faust, Yutaka Matsuo, Percy Liang, and Sherry Yang. Improving dynamic object interactions in text-to-video generation with ai feedback. *arXiv preprint arXiv:2412.02617*, 2024.
- [16] Ruiqi Gao, Emiel Hoogeboom, Jonathan Heek, Valentin De Bortoli, Kevin P. Murphy, and Tim Salimans. Diffusion meets flow matching: Two sides of the same coin. 2024. URL <https://diffusionflow.github.io/>.
- [17] Dhruva Ghosh, Hannaneh Hajishirzi, and Ludwig Schmidt. Geneval: An object-focused framework for evaluating text-to-image alignment. *Advances in Neural Information Processing Systems*, 36:52132–52152, 2023.
- [18] Daya Guo, Dejian Yang, Haowei Zhang, Junxiao Song, Ruoyu Zhang, Runxin Xu, Qihao Zhu, Shirong Ma, Peiyi Wang, Xiao Bi, et al. Deepseek-r1: Incentivizing reasoning capability in llms via reinforcement learning. *arXiv preprint arXiv:2501.12948*, 2025.
- [19] Dong Guo, Faming Wu, Feida Zhu, Fuxing Leng, Guang Shi, Haobin Chen, Haoqi Fan, Jian Wang, Jianyu Jiang, Jiawei Wang, et al. Seed1. 5-vl technical report. *arXiv preprint arXiv:2505.07062*, 2025.
- [20] Shashank Gupta, Chaitanya Ahuja, Tsung-Yu Lin, Sreya Dutta Roy, Harrie Oosterhuis, Maarten de Rijke, and Satya Narayan Shukla. A simple and effective reinforcement learning method for text-to-image diffusion fine-tuning. *arXiv preprint arXiv:2503.00897*, 2025.
- [21] Jonathan Ho and Tim Salimans. Classifier-free diffusion guidance, 2022. URL <https://arxiv.org/abs/2207.12598>.
- [22] Jonathan Ho, Ajay Jain, and Pieter Abbeel. Denoising diffusion probabilistic models. *Advances in neural information processing systems*, 33:6840–6851, 2020.
- [23] Jian Hu, Jason Klein Liu, Haotian Xu, and Wei Shen. Reinforce++: An efficient rlhf algorithm with robustness to both prompt and reward models. *arXiv preprint arXiv:2501.03262*, 2025.
- [24] Kaiyi Huang, Kaiyue Sun, Enze Xie, Zhenguo Li, and Xihui Liu. T2i-compbench: A comprehensive benchmark for open-world compositional text-to-image generation. *Advances in Neural Information Processing Systems*, 36:78723–78747, 2023.
- [25] Aaron Jaech, Adam Kalai, Adam Lerer, Adam Richardson, Ahmed El-Kishky, Aiden Low, Alec Helyar, Aleksander Madry, Alex Beutel, Alex Carney, et al. Openai o1 system card. *arXiv preprint arXiv:2412.16720*, 2024.
- [26] Sham M Kakade. A natural policy gradient. *Advances in neural information processing systems*, 14, 2001.
- [27] Yuval Kirstain, Adam Polyak, Uriel Singer, Shahbuland Matiana, Joe Penna, and Omer Levy. Pick-a-pic: An open dataset of user preferences for text-to-image generation. *Advances in neural information processing systems*, 36:36652–36663, 2023.
- [28] Vijay R Konda and John N Tsitsiklis. Onactor-critic algorithms. *SIAM journal on Control and Optimization*, 42(4):1143–1166, 2003.
- [29] Nathan Lambert, Jacob Morrison, Valentina Pyatkin, Shengyi Huang, Hamish Ivison, Faeze Brahman, Lester James V Miranda, Alisa Liu, Nouha Dziri, Shane Lyu, et al. Tulu 3: Pushing frontiers in open language model post-training. *arXiv preprint arXiv:2411.15124*, 2024.

- [30] Kimin Lee, Hao Liu, Moonkyung Ryu, Olivia Watkins, Yuqing Du, Craig Boutilier, Pieter Abbeel, Mohammad Ghavamzadeh, and Shixiang Shane Gu. Aligning text-to-image models using human feedback. *arXiv preprint arXiv:2302.12192*, 2023.
- [31] Junnan Li, Dongxu Li, Caiming Xiong, and Steven Hoi. Blip: Bootstrapping language-image pre-training for unified vision-language understanding and generation. In *ICML*, 2022.
- [32] Junzhe Li, Yutao Cui, Tao Huang, Yinping Ma, Chun Fan, Miles Yang, and Zhao Zhong. Mixgrpo: Unlocking flow-based grpo efficiency with mixed ode-sde, 2025. URL <https://arxiv.org/abs/2507.21802>.
- [33] Shufan Li, Konstantinos Kallidromitis, Akash Gokul, Yusuke Kato, and Kazuki Kozuka. Aligning diffusion models by optimizing human utility. *Advances in Neural Information Processing Systems*, 37:24897–24925, 2024.
- [34] Yuming Li, Yikai Wang, Yuying Zhu, Zhongyu Zhao, Ming Lu, Qi She, and Shanghang Zhang. Branchgrpo: Stable and efficient grpo with structured branching in diffusion models. *arXiv preprint arXiv:2509.06040*, 2025.
- [35] Ziniu Li, Tian Xu, Yushun Zhang, Zhihang Lin, Yang Yu, Ruoyu Sun, and Zhi-Quan Luo. Remax: A simple, effective, and efficient reinforcement learning method for aligning large language models. *arXiv preprint arXiv:2310.10505*, 2023.
- [36] Zhanhao Liang, Yuhui Yuan, Shuyang Gu, Bohan Chen, Tiankai Hang, Mingxi Cheng, Ji Li, and Liang Zheng. Aesthetic post-training diffusion models from generic preferences with step-by-step preference optimization. In *Proceedings of the Computer Vision and Pattern Recognition Conference*, pages 13199–13208, 2025.
- [37] Zhengyang Liang, Hao He, Ceyuan Yang, and Bo Dai. Scaling laws for diffusion transformers. *arXiv preprint arXiv:2410.08184*, 2024.
- [38] Timothy P Lillicrap, Jonathan J Hunt, Alexander Pritzel, Nicolas Heess, Tom Erez, Yuval Tassa, David Silver, and Daan Wierstra. Continuous control with deep reinforcement learning. *arXiv preprint arXiv:1509.02971*, 2015.
- [39] Shanchuan Lin, Xin Xia, Yuxi Ren, Ceyuan Yang, Xuefeng Xiao, and Lu Jiang. Diffusion adversarial post-training for one-step video generation. *arXiv preprint arXiv:2501.08316*, 2025.
- [40] Yaron Lipman, Ricky T. Q. Chen, Heli Ben-Hamu, Maximilian Nickel, and Matthew Le. Flow matching for generative modeling. In *The Eleventh International Conference on Learning Representations*, 2023. URL <https://openreview.net/forum?id=PqvMRDCJT9t>.
- [41] Yaron Lipman, Marton Havasi, Peter Holderrieth, Neta Shaul, Matt Le, Brian Karrer, Ricky T. Q. Chen, David Lopez-Paz, Heli Ben-Hamu, and Itai Gat. Flow matching guide and code, 2024. URL <https://arxiv.org/abs/2412.06264>.
- [42] Jiashun Liu, Johan Obando-Ceron, Han Lu, Yancheng He, Weixun Wang, Wenbo Su, Bo Zheng, Pablo Samuel Castro, Aaron Courville, and Ling Pan. Asymmetric proximal policy optimization: mini-critics boost llm reasoning. *arXiv preprint arXiv:2510.01656*, 2025.
- [43] Jie Liu, Gongye Liu, Jiajun Liang, Yangguang Li, Jiaheng Liu, Xintao Wang, Pengfei Wan, Di ZHANG, and Wanli Ouyang. Flow-GRPO: Training flow matching models via online RL. In *The Thirty-ninth Annual Conference on Neural Information Processing Systems*, 2025. URL <https://openreview.net/forum?id=oCBKGw5HNf>.
- [44] Runtao Liu, Haoyu Wu, Ziqiang Zheng, Chen Wei, Yingqing He, Renjie Pi, and Qifeng Chen. Videodpo: Omni-preference alignment for video diffusion generation. In *Proceedings of the Computer Vision and Pattern Recognition Conference*, pages 8009–8019, 2025.
- [45] Xingchao Liu, Chengyue Gong, and qiang liu. Flow straight and fast: Learning to generate and transfer data with rectified flow. In *The Eleventh International Conference on Learning Representations*, 2023. URL <https://openreview.net/forum?id=XVjTT1nw5z>.

- [46] Ilya Loshchilov and Frank Hutter. Decoupled weight decay regularization. In *International Conference on Learning Representations*, 2019. URL <https://openreview.net/forum?id=Bkg6RiCqY7>.
- [47] Yuhang Ma, Xiaoshi Wu, Keqiang Sun, and Hongsheng Li. Hpsv3: Towards wide-spectrum human preference score. In *Proceedings of the IEEE/CVF International Conference on Computer Vision*, pages 15086–15095, 2025.
- [48] David McAllister, Songwei Ge, Brent Yi, Chung Min Kim, Ethan Weber, Hongsuk Choi, Haiwen Feng, and Angjoo Kanazawa. Flow matching policy gradients, 2025. URL <https://arxiv.org/abs/2507.21053>.
- [49] Zichen Miao, Jiang Wang, Ze Wang, Zhengyuan Yang, Lijuan Wang, Qiang Qiu, and Zicheng Liu. Training diffusion models towards diverse image generation with reinforcement learning. In *Proceedings of the IEEE/CVF Conference on Computer Vision and Pattern Recognition*, pages 10844–10853, 2024.
- [50] Volodymyr Mnih, Adria Puigdomenech Badia, Mehdi Mirza, Alex Graves, Timothy Lillicrap, Tim Harley, David Silver, and Koray Kavukcuoglu. Asynchronous methods for deep reinforcement learning. In *International conference on machine learning*, pages 1928–1937. PmLR, 2016.
- [51] Long Ouyang, Jeffrey Wu, Xu Jiang, Diogo Almeida, Carroll Wainwright, Pamela Mishkin, Chong Zhang, Sandhini Agarwal, Katarina Slama, Alex Ray, et al. Training language models to follow instructions with human feedback. *Advances in neural information processing systems*, 35:27730–27744, 2022.
- [52] William Peebles and Saining Xie. Scalable diffusion models with transformers. In *Proceedings of the IEEE/CVF international conference on computer vision*, pages 4195–4205, 2023.
- [53] Xue Bin Peng, Aviral Kumar, Grace Zhang, and Sergey Levine. Advantage-weighted regression: Simple and scalable off-policy reinforcement learning. *arXiv preprint arXiv:1910.00177*, 2019.
- [54] Mihir Prabhudesai, Anirudh Goyal, Deepak Pathak, and Katerina Fragkiadaki. Aligning text-to-image diffusion models with reward backpropagation, 2023.
- [55] Mihir Prabhudesai, Russell Mendonca, Zheyang Qin, Katerina Fragkiadaki, and Deepak Pathak. Video diffusion alignment via reward gradients, 2024. URL <https://arxiv.org/abs/2407.08737>.
- [56] Alec Radford, Jong Wook Kim, Chris Hallacy, Aditya Ramesh, Gabriel Goh, Sandhini Agarwal, Girish Sastry, Amanda Askell, Pamela Mishkin, Jack Clark, et al. Learning transferable visual models from natural language supervision. In *International conference on machine learning*, pages 8748–8763. PmLR, 2021.
- [57] Rafael Rafailov, Archit Sharma, Eric Mitchell, Christopher D Manning, Stefano Ermon, and Chelsea Finn. Direct preference optimization: Your language model is secretly a reward model. *Advances in neural information processing systems*, 36:53728–53741, 2023.
- [58] John Schulman, Sergey Levine, Pieter Abbeel, Michael Jordan, and Philipp Moritz. Trust region policy optimization. In *International conference on machine learning*, pages 1889–1897. PMLR, 2015.
- [59] John Schulman, Philipp Moritz, Sergey Levine, Michael Jordan, and Pieter Abbeel. High-dimensional continuous control using generalized advantage estimation. In *Proceedings of the International Conference on Learning Representations (ICLR)*, 2016.
- [60] John Schulman, Filip Wolski, Prafulla Dhariwal, Alec Radford, and Oleg Klimov. Proximal policy optimization algorithms. *arXiv preprint arXiv:1707.06347*, 2017.
- [61] Team Seaweed, Ceyuan Yang, Zhijie Lin, Yang Zhao, Shanchuan Lin, Zhibei Ma, Haoyuan Guo, Hao Chen, Lu Qi, Sen Wang, et al. Seaweed-7b: Cost-effective training of video generation foundation model. *arXiv preprint arXiv:2504.08685*, 2025.

- [62] ByteDance Seed, Jiaze Chen, Tiantian Fan, Xin Liu, Lingjun Liu, Zhiqi Lin, Mingxuan Wang, Chengyi Wang, Xiangpeng Wei, Wenyuan Xu, et al. Seed1. 5-thinking: Advancing superb reasoning models with reinforcement learning. *arXiv preprint arXiv:2504.13914*, 2025.
- [63] Zhihong Shao, Peiyi Wang, Qihao Zhu, Runxin Xu, Junxiao Song, Xiao Bi, Haowei Zhang, Mingchuan Zhang, YK Li, Yang Wu, et al. Deepseekmath: Pushing the limits of mathematical reasoning in open language models. *arXiv preprint arXiv:2402.03300*, 2024.
- [64] Dingyuan Shi, Yong Wang, Hangyu Li, and Xiangxiang Chu. Preference alignment for diffusion model via explicit denoised distribution estimation. *arXiv preprint arXiv:2411.14871*, 2024.
- [65] David Silver, Guy Lever, Nicolas Heess, Thomas Degris, Daan Wierstra, and Martin Riedmiller. Deterministic policy gradient algorithms. In Eric P. Xing and Tony Jebara, editors, *Proceedings of the 31st International Conference on Machine Learning*, volume 32 of *Proceedings of Machine Learning Research*, pages 387–395, Beijing, China, 22–24 Jun 2014. PMLR. URL <https://proceedings.mlr.press/v32/silver14.html>.
- [66] Raghav Singhal, Zachary Horvitz, Ryan Teehan, Mengye Ren, Zhou Yu, Kathleen McKeown, and Rajesh Ranganath. A general framework for inference-time scaling and steering of diffusion models. In *Forty-second International Conference on Machine Learning*, 2025. URL <https://openreview.net/forum?id=Jp988ELppQ>.
- [67] Jiaming Song, Chenlin Meng, and Stefano Ermon. Denoising diffusion implicit models. In *International Conference on Learning Representations*, 2021. URL <https://openreview.net/forum?id=St1giarCHLP>.
- [68] Yang Song and Stefano Ermon. Generative modeling by estimating gradients of the data distribution. *Advances in neural information processing systems*, 32, 2019.
- [69] Yang Song, Jascha Sohl-Dickstein, Diederik P Kingma, Abhishek Kumar, Stefano Ermon, and Ben Poole. Score-based generative modeling through stochastic differential equations. *arXiv preprint arXiv:2011.13456*, 2020.
- [70] Nisan Stiennon, Long Ouyang, Jeffrey Wu, Daniel Ziegler, Ryan Lowe, Chelsea Voss, Alec Radford, Dario Amodei, and Paul F Christiano. Learning to summarize with human feedback. *Advances in neural information processing systems*, 33:3008–3021, 2020.
- [71] Kimi Team, Angang Du, Bofei Gao, Bowei Xing, Changjiu Jiang, Cheng Chen, Cheng Li, Chenjun Xiao, Chenzhuang Du, Chonghua Liao, et al. Kimi k1. 5: Scaling reinforcement learning with llms. *arXiv preprint arXiv:2501.12599*, 2025.
- [72] Yibin Wang, Yuhang Zang, Hao Li, Cheng Jin, and Jiaqi Wang. Unified reward model for multimodal understanding and generation. *arXiv preprint arXiv:2503.05236*, 2025.
- [73] Ronald J Williams. Simple statistical gradient-following algorithms for connectionist reinforcement learning. *Machine learning*, 8(3):229–256, 1992.
- [74] Chenfei Wu, Jiahao Li, Jingren Zhou, Junyang Lin, Kaiyuan Gao, Kun Yan, Sheng-ming Yin, Shuai Bai, Xiao Xu, Yilei Chen, et al. Qwen-image technical report. *arXiv preprint arXiv:2508.02324*, 2025.
- [75] Luhuan Wu, Brian L Trippe, Christian Naesseth, David Blei, and John P Cunningham. Practical and asymptotically exact conditional sampling in diffusion models. *Advances in Neural Information Processing Systems*, 2023.
- [76] Xiaoshi Wu, Yiming Hao, Keqiang Sun, Yixiong Chen, Feng Zhu, Rui Zhao, and Hongsheng Li. Human preference score v2: A solid benchmark for evaluating human preferences of text-to-image synthesis. *arXiv preprint arXiv:2306.09341*, 2023.
- [77] Xiaoshi Wu, Keqiang Sun, Feng Zhu, Rui Zhao, and Hongsheng Li. Human preference score: Better aligning text-to-image models with human preference. In *Proceedings of the IEEE/CVF International Conference on Computer Vision*, pages 2096–2105, 2023.

- [78] Ziyi Wu, Anil Kag, Ivan Skorokhodov, Willi Menapace, Ashkan Mirzaei, Igor Gilitschenski, Sergey Tulyakov, and Aliaksandr Siarohin. DenseDPO: Fine-grained temporal preference optimization for video diffusion models. *NeurIPS*, 2025.
- [79] Jiazheng Xu, Xiao Liu, Yuchen Wu, Yuxuan Tong, Qinkai Li, Ming Ding, Jie Tang, and Yuxiao Dong. Imagereward: Learning and evaluating human preferences for text-to-image generation. *Advances in Neural Information Processing Systems*, 36:15903–15935, 2023.
- [80] Shuchen Xue, Chongjian Ge, Shilong Zhang, Yichen Li, and Zhi-Ming Ma. Advantage weighted matching: Aligning rl with pretraining in diffusion models. *arXiv preprint arXiv:2509.25050*, 2025.
- [81] Zeyue Xue, Jie Wu, Yu Gao, Fangyuan Kong, Lingting Zhu, Mengzhao Chen, Zhiheng Liu, Wei Liu, Qiushan Guo, Weilin Huang, et al. Dancegrpo: Unleashing grpo on visual generation. *arXiv preprint arXiv:2505.07818*, 2025.
- [82] Kai Yang, Jian Tao, Jiafei Lyu, Chunjiang Ge, Jiabin Chen, Weihang Shen, Xiaolong Zhu, and Xiu Li. Using human feedback to fine-tune diffusion models without any reward model. In *Proceedings of the IEEE/CVF Conference on Computer Vision and Pattern Recognition*, pages 8941–8951, 2024.
- [83] Shentao Yang, Tianqi Chen, and Mingyuan Zhou. A dense reward view on aligning text-to-image diffusion with preference. *arXiv preprint arXiv:2402.08265*, 2024.
- [84] Yuanyang Yin, Yaqi Zhao, Mingwu Zheng, Ke Lin, Jiarong Ou, Rui Chen, Victor Sheajay Huang, Jiahao Wang, Xin Tao, Pengfei Wan, et al. Towards precise scaling laws for video diffusion transformers. In *Proceedings of the Computer Vision and Pattern Recognition Conference*, pages 18155–18165, 2025.
- [85] Huizhuo Yuan, Zixiang Chen, Kaixuan Ji, and Quanquan Gu. Self-play fine-tuning of diffusion models for text-to-image generation. *Advances in Neural Information Processing Systems*, 37: 73366–73398, 2024.
- [86] Chuheng Zhang, Wei Shen, Li Zhao, Xuyun Zhang, Xiaolong Xu, Wanchun Dou, and Jiang Bian. Policy filtration for RLHF to mitigate noise in reward models. In *Forty-second International Conference on Machine Learning*, 2025. URL <https://openreview.net/forum?id=L8hYdTQVcs>.
- [87] Jiacheng Zhang, Jie Wu, Weifeng Chen, Yatai Ji, Xuefeng Xiao, Weilin Huang, and Kai Han. Onlinevpo: Align video diffusion model with online video-centric preference optimization. *arXiv preprint arXiv:2412.15159*, 2024.
- [88] Tao Zhang, Cheng Da, Kun Ding, Huan Yang, kun jin, Yan Li, Tingting Gao, Di ZHANG, Shiming Xiang, and Chunhong Pan. Diffusion model as a noise-aware latent reward model for step-level preference optimization. In *The Thirty-ninth Annual Conference on Neural Information Processing Systems*, 2025. URL <https://openreview.net/forum?id=YB9VGCC1v9>.
- [89] Xiangcheng Zhang, Haowei Lin, Haotian Ye, James Zou, Jianzhu Ma, Yitao Liang, and Yilun Du. Inference-time scaling of diffusion models through classical search. *arXiv preprint arXiv:2505.23614*, 2025.
- [90] Yinan Zhang, Eric Tzeng, Yilun Du, and Dmitry Kislyuk. Large-scale reinforcement learning for diffusion models. In *European Conference on Computer Vision*, pages 1–17. Springer, 2024.
- [91] Hanyang Zhao, Haoxian Chen, Ji Zhang, David Yao, and Wenpin Tang. Score as action: Fine tuning diffusion generative models by continuous-time reinforcement learning. In *Forty-second International Conference on Machine Learning*, 2025. URL <https://openreview.net/forum?id=V5HEX6stS2>.
- [92] Chujie Zheng, Shixuan Liu, Mingze Li, Xiong-Hui Chen, Bowen Yu, Chang Gao, Kai Dang, Yuqiong Liu, Rui Men, An Yang, et al. Group sequence policy optimization. *arXiv preprint arXiv:2507.18071*, 2025.

- [93] Yujie Zhou, Pengyang Ling, Jiazi Bu, Yibin Wang, Yuhang Zang, Jiaqi Wang, Li Niu, and Guangtao Zhai. Fine-grained grpo for precise preference alignment in flow models, 2025. URL <https://arxiv.org/abs/2510.01982>.
- [94] Dingwei Zhu, Shihan Dou, Zhiheng Xi, Senjie Jin, Guoqiang Zhang, Jiazheng Zhang, Junjie Ye, Mingxu Chai, Enyu Zhou, Ming Zhang, Caishuang Huang, Yunke Zhang, Yuran Wang, and Tao Gui. Vrpo: Rethinking value modeling for robust rl training under noisy supervision, 2025. URL <https://arxiv.org/abs/2508.03058>.

A Appendix Overview

This appendix is organized as follows:

- Section B discusses the limitations of our approach.
- Section C summarizes the notation used throughout the paper.
- Section D reviews additional related work.
- Section E reports further results on inference-time steering.
- Section F provides additional implementation and methodological details.
- Section G shows additional visual results and comparisons.

B Limitations

Our approach still has several limitations. First, we focus exclusively on image diffusion models; extending our actor-critic framework to video or other modalities remains an open challenge. Second, although our multi-value-head design supports multi-reward optimization, the optimization efficiency for each individual reward can degrade compared to single-reward training. Third, our method relies on time discretization when sampling from the SDE, which may introduce discretization error and limit the RL efficiency. We leave these directions for future work.

C Notation

Table 7 summarizes the notation and abbreviations used in this paper.

D Extended Related Work

Credit assignment in diffusion RL. A central challenge in diffusion RL is credit assignment along the denoising trajectory: rewards are typically observed only on the final decoded image, while optimization must assign credit to intermediate denoising steps. Existing methods address this problem in different ways. Early RL-based approaches such as DDPO and DPDK mainly optimize terminal rewards with policy gradients [4, 14]. Preference-based methods have explored denser or step-aware supervision, for example through temporal discounting [83], step-aware preference optimization [36], and explicit denoised-distribution estimation that links intermediate steps to the final denoised outcome [64]. Within the GRPO family, current work avoids explicit value learning and instead relies on relative group signals for trajectory optimization [43, 81]. More recent follow-up work pushes this direction further with finer-grained reward assignment, including granular reward assessment in G²RPO, dense step-wise rewards in DenseGRPO, and tree-structured temporal credit assignment in TreeGRPO [93, 7, 9]. Our work is complementary to these approaches: instead of redesigning relative or dense reward signals, we learn an explicit critic for trajectory-level actor-critic optimization.

Representation and state-space alignment. Another underexplored issue is the representation space in which alignment signals are defined. Many existing diffusion alignment pipelines evaluate decoded images with external reward models or vision-language encoders even when optimization concerns intermediate denoising states [91, 4]. This creates a mismatch between the states visited by the policy and the states evaluated by the reward model or critic. Several recent works begin to address this issue more directly. SPO introduces step-aware preference modeling at each denoising step [36]; DDE explicitly connects intermediate states to the terminal denoised distribution for preference alignment [64]; and LPO argues that diffusion backbones are naturally suited for modeling rewards directly on noisy latent states [88]. These works move toward diffusion-native representations, but they do not learn an explicit value critic for online actor-critic optimization. Our work shares the same intuition that alignment signals should be defined in the noisy latent space, but uses this representation to learn a timestep-conditioned value function so that actor and critic operate in the same state space.

Diffusion/Flow Models. Diffusion-based generative models have achieved state-of-the-art performance in visual synthesis. Denoising diffusion probabilistic models (DDPMs) [22] formulate

Symbol	Meaning	Symbol	Meaning
x_0	Clean data sample (image latent).	s_k	State at step k , e.g. (x_{t_k}, t_k, y) .
x_t	Noisy latent at time t .	a_k	Action at step k (predicted denoising direction).
x_1	Standard normal latent in OT-path flow matching.	r_k	Reward at step k (zero for $k < T$, terminal-only at $k = T$).
t, t_k	Continuous time or discrete timestep.	R_k	Return-to-go $\sum_{l=0}^{T-k} \gamma^l r_{k+l}$.
T	Number of reverse-diffusion / flow steps.	A_k	Advantage estimate at step k .
y	Text prompt / conditioning input.	$V_\phi(s_k)$	Value function (critic) at state s_k .
$v_\theta(x_t, t)$	Policy / flow network prediction (velocity / noise).	δ_k	TD residual $r_k + \gamma V_\phi(s_{k+1}) - V_\phi(s_k)$.
\hat{x}_0, \hat{x}_1	Reconstructions used in the stochastic flow sampler.	γ	Discount factor in RL.
Δt	Step size between adjacent time steps.	λ	GAE parameter (bias–variance trade-off).
ϵ	Standard Gaussian noise, $\epsilon \sim \mathcal{N}(0, I)$.	$\pi_\theta(a_k s_k, t_k)$	Stochastic policy at step k .
σ_t	Noise scale / stochasticity at time t .	π_{ref}	Frozen pretrained reference policy.
$\alpha_t, \bar{\alpha}_t$	DDPM schedule, $\bar{\alpha}_t = \prod_{s=1}^t \alpha_s$.	$r_k(\theta)$	Policy likelihood ratio $\frac{\pi_\theta(a_k s_k, t_k)}{\pi_{\theta_{\text{old}}}(a_k s_k, t_k)}$ in PPO.
$v(x_t, t)$	Ground-truth OT-path velocity $x_1 - x_0$.	$J(\theta)$	Expected return.
\mathcal{T}_t	One-step sampler transition (DDIM / Euler).	τ	Trajectory $\{x_{t_k}\}_{k=0}^T$.
K	Number of particles in SMC.	$x_t^{(i)}$	i -th particle in SMC at time t .
$w_t^{(i)}$	Normalized weight of particle i in SMC.	g_t	Critic gradient $\nabla_{x_t} V_\phi(x_t, t, y)$ for guidance.
η	Guidance scale for critic-based steering.		
PPO	Proximal Policy Optimization.	GAE	Generalized Advantage Estimation.
MDP	Markov Decision Process.	BoN	Best-of- N sampling baseline.
SMC	Sequential Monte Carlo sampling.	UNet	U-shaped convolutional backbone.
DiT	Diffusion Transformer backbone.	VAE	Variational Autoencoder.
HPS	Human Preference Score (HPSv2.1).	OCR	Optical Character Recognition reward.
SD1.5	Stable Diffusion 1.5 backbone.	SD3.5M	Stable Diffusion 3.5M backbone.

Table 7: **Summary of the notation and abbreviations used in this paper.**

generation as reversing a fixed Markovian noising process and optimize a variational bound that can be interpreted as denoising score matching [68]. Score-based diffusion models further generalize this view by describing the forward and reverse processes as stochastic differential equations and learning time-dependent score functions, which yields a unified framework for diffusion and Langevin-based samplers and enables powerful conditional generation for diverse vision tasks [69]. Flow-matching models directly learning continuous-time vector fields that transport a simple prior to the data distribution within the framework of continuous normalizing flows [40, 45]. Recent analyses show that Gaussian flow matching and diffusion models are closely related and can be viewed as two parameterizations of the same underlying continuous-time generative process, offering complementary design choices in terms of objective, architecture, and discretization [41, 16]. In practice, flow-matching models have emerged as an attractive alternative for building fast, high-fidelity generative priors for modern vision applications.

Post-training for Foundation Models. Foundation models are typically obtained by large-scale pre-training on generic corpora, and then adapted to downstream use via a post-training pipeline. Modern post-training stacks begin with supervised instruction tuning on curated demonstrations to teach the model task formats and high-level alignment objectives [51]. On top of this, reinforcement learning from human feedback (RLHF) trains a reward model from pairwise preferences and then optimizes the policy with reinforcement learning (e.g., PPO), improving helpfulness, safety, and calibration beyond pure supervised learning [2, 29]. To reduce dependence on expensive human labels, recent work explores reinforcement learning from AI feedback [3] (RLAIF) and reinforce-

ment learning with verifiable rewards (RLVR) [63, 71], where the reward signal is derived from automatically checkable criteria such as unit tests, program analyzers, or self-consistency checks, making it particularly suitable for code generation and long-horizon reasoning tasks. In parallel, direct preference optimization objectives such as DPO and related methods bypass explicit reward modeling and directly fit the policy to preference data while regularizing towards the pre-trained model [57]. Recent reasoning-centric foundation models, including the OpenAI o1 [25] series and DeepSeek-R1 [18], instantiate multi-stage post-training pipelines that combine large-scale instruction tuning, RLHF-/RLVR-style optimization, and process-level supervision over chain-of-thought traces, yielding substantial gains on math, coding, and scientific reasoning benchmarks. Overall, instruction tuning, RLHF/RLAIF, RLVR-style verifiable-reward training, and direct preference optimization have emerged as the main families of post-training methods for aligning general-purpose foundation models with target tasks and user preferences.

RL with Critics for LLM Post-training A large fraction of RL post-training for language models follows a critic-based design, where a value function is learned jointly with the policy to handle sparse, sequence-level feedback. In RLHF pipelines such as InstructGPT [51] and Constitutional AI [3], a reward model is first trained from human or AI preferences, and PPO with a value head on the LM is then used to maximize the reward under KL regularization [94]. Similar architectures appear in RL with verifiable or tool-based rewards, where the critic must propagate terminal signals back through long action sequences [42, 13]. Recent work shows that careful choices of value normalization, credit assignment, and trajectory filtering allow PPO-style critics to scale to harder reasoning and long chain-of-thought settings [85, 62, 19, 86]. These results suggest that strong, well-trained critics remain central when we need high performance on complex generation tasks; our work follows this line but adapts the value architecture and training to the latent, multi-step structure of diffusion models.

Policy Gradient Methods. Policy-gradient methods optimize a parameterized policy by directly ascending the gradient of the expected return, rather than relying on value-based bootstrapping. Early work such as REINFORCE [73] established the likelihood-ratio estimator and showed that subtracting a learned baseline can substantially reduce gradient variance. Actor-critic architectures extend this idea by coupling a policy (actor) with a learned value function (critic), enabling more sample-efficient and stable learning in both continuous and discrete control [28, 50]. Building on the natural policy gradient [26], trust-region methods such as TRPO [58] constrain policy updates within a KL-divergence trust region to prevent catastrophic performance collapse, while generalized advantage estimation further improves the bias–variance trade-off of the policy-gradient estimator [59]. Proximal Policy Optimization (PPO) simplifies TRPO by replacing hard trust-region constraints with clipped surrogate objectives, yielding a robust and computationally efficient on-policy algorithm that has become the de facto choice in many large-scale RL applications [60]. In parallel, deterministic policy-gradient methods and their deep variants (e.g., DDPG) extend policy-gradient ideas to off-policy learning in continuous action spaces via critic-based Q-function estimation and target networks [65, 38]. These developments form the algorithmic backbone for modern reinforcement-learning-based post-training of foundation models, where PPO-style policy gradients, variance-reduced advantage estimation, and critic-based shaping are widely used to optimize reward models derived from human or verifiable feedback.

E More Results on Inference Time Steering

In this section, we provide more inference time steering results on CLIP and PickScore. The results are shown in Fig. 9. We can observe that critic guidance can consistently improve on baseline and BoN.

F Details

F.1 Training Details

Optimization. We use AdamW [46] to optimize both the policy and value networks in all experiments. The momentum coefficients are set to $(\beta_1, \beta_2) = (0.9, 0.95)$ and the weight decay is 1×10^{-4} . The policy learning rate is fixed to 1×10^{-4} across all settings for a fair comparison. Each run is trained for 300 iterations, and every iteration consists of 4 gradient update steps.

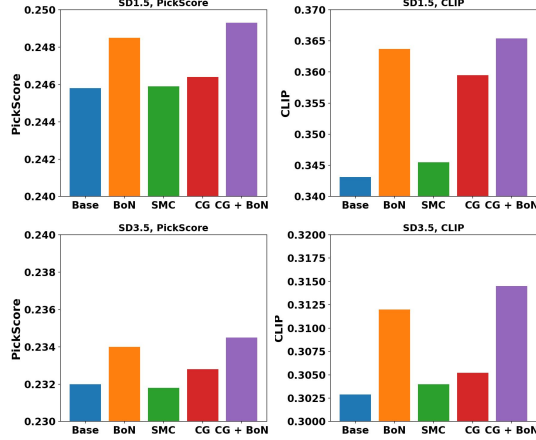


Figure 9: Inference steering results on CLIP and PickScore.

SD1.5. For SD1.5 experiments, we draw a large batch of 3,840 images per iteration. Given 4 update steps, the effective batch size per gradient update is $3840/4 = 960$ samples. The PPO ratio clipping range is set to 1×10^{-5} . We clip the advantages to the range $[-10, 10]$ and the value targets to $[-5, 5]$. The learning rate of the value network is 1×10^{-4} . Experiments on SD1.5 require 8 H100 GPUs.

SD3.5M. For SD3.5M experiments, we sample 384 images per iteration for the human-preference reward and the CLIP-based reward. For other non-differentiable rewards, we use a larger batch of 3,840 samples. Empirically, we find that small batch sizes lead to unstable training for DDPO/GRPO-style updates, hence the larger batch is beneficial in this case. The ratio clipping range is set to 1×10^{-4} . We keep the same advantage clipping range $[-10, 10]$ and value clipping range $[-5, 5]$. The value network learning rate is set to 1×10^{-3} . Experiments on SD1.5 require 32 H100 GPUs.

Sampling. During training, the sampling configuration is aligned with that used at inference time. For SD1.5, we use the DDIM [67] sampler with 50 diffusion steps. For SD3.5M, we use the Discrete Euler sampler with 40 steps. Unless otherwise specified, classifier-free guidance is disabled in all experiments.

Normalization. After computing the per-sample advantages, we apply advantage normalization over the global batch. Concretely, we compute the mean and standard deviation of all advantages in the batch and normalize as

$$A_k = \frac{A_k - A_{\text{mean}}}{A_{\text{std}}}. \quad (6)$$

We do not apply any additional normalization to rewards or value targets.

Inference Details At inference time, we use the same sampling configurations as in the training phase. For SD1.5 models, we employ DDIM with 50 sampling steps. For SD3.5M models, we use the Discrete Euler sampler with 40 steps. Classifier-free guidance is disabled for all reported results.

Multiple Reward Experiment Details To support multiple reward signals, we implement a unified dataset that manages several prompt sets corresponding to different rewards. At each training iteration, we sample prompts from these datasets according to the proportions specified in the configuration. Each returned data item contains the following fields: reward type, prompt, weight, and metadata. The metadata field is empty for human-preference rewards. For GenEval, it encodes the required number of objects or the target color. For OCR text-rendering rewards, it stores the desired characters that should appear in the generated image. By assigning different weights to different reward types, we can balance their relative contributions to the overall learning signal.

Critic Attention Layers We augment the diffusion transformer with critic attention layers inserted at layers 7, 15, and 23. Each critic attention layer contains a single learnable query token that aggregates information from the intermediate visual tokens. After passing through all critic attention layers, we

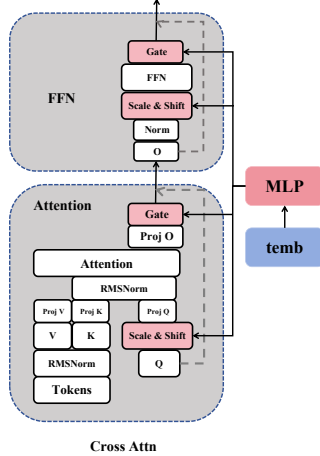


Figure 10: Architecture of the critic attention layer.

concatenate the resulting query tokens and project them to a scalar prediction, which serves as the value estimate.

Within each critic attention layer, the visual tokens are first processed by an RMSNorm. We then obtain the query, key, and value projections (Q/K/V). Before feeding them into the attention module, we apply QKNorm to Q and K to improve numerical stability. The attention module produces a single output token corresponding to the learned query. This token is further processed by a feed-forward network (FFN) to refine the value representation.

Time Conditioning We empirically find that incorporating the diffusion timestep is crucial for the critic. We therefore adopt an adaptive layer-normalization (AdaLN) style time conditioning in the critic attention layers. Specifically, the learned diffusion time embedding is first processed by an MLP to produce per-channel *scale*, *shift*, and *gate* coefficients. The learnable query token is scaled and shifted before the RMSNorm using the corresponding coefficients. After the attention operation, the output token is gated by the residual input using the gate coefficient. The MLP also produces scale, shift, and gate coefficients for modulating the FFN. The overall architecture of the critic attention layer and its time conditioning is illustrated in Fig. 10.

F.2 GAE

We use generalized advantage estimation (GAE) to compute the advantages for policy updates. Given a trajectory $\{(s_t, a_t, r_t)\}_{t=0}^T$, we first compute the temporal-difference (TD) residuals

$$\delta_t = r_t + \gamma V_\phi(s_{t+1}) - V_\phi(s_t), \quad (7)$$

where V_ϕ denotes the value network, and we set $V_\phi(s_{T+1}) = 0$ for terminal states. The GAE advantage at time step t is then defined as

$$A_t^{\text{GAE}} = \sum_{l=0}^{T-t-1} (\gamma\lambda)^l \delta_{t+l}. \quad (8)$$

GAE involves two hyperparameters: the discount factor γ and the decay factor λ . The discount factor $\gamma \in [0, 1]$ controls how strongly future rewards are taken into account; smaller values emphasize immediate rewards. The decay factor $\lambda \in [0, 1]$ governs the bias-variance trade-off of the estimator: $\lambda = 0$ corresponds to a TD(0)-style estimate with higher bias but lower variance, whereas $\lambda = 1$ recovers the Monte-Carlo return with lower bias but higher variance.

In our setting, trajectories are short, and the reward is provided at the end of the trajectory. We therefore set both hyperparameters to $\gamma = 1$ and $\lambda = 1$ in all experiments, which reduces GAE to an undiscounted Monte-Carlo estimator of the advantages. After computing A_t^{GAE} , we apply the global advantage normalization described above.

F.3 Reward Models

In our experiments, we employ five reward models: CLIP, HPSv2.1, PickScore, GenEval, and OCR. All of them take the generated image, the associated prompt, and additional metadata as input and output a scalar score, which we directly use as the reward without extra normalization.

CLIP [56]. CLIP measures the text-image alignment between a generated image and its corresponding prompt. Concretely, we encode the prompt and the image with a pretrained CLIP text encoder and image encoder, and compute the cosine similarity between the resulting embeddings. This similarity serves as the CLIP reward, encouraging the model to generate images that are semantically aligned with the input text. We use ViT-L-14 variant in our experiments.

HPSv2.1 [76]. HPSv2.1 is a human-preference score model trained on large-scale human annotations. Given a prompt and an image, it predicts how likely a human would prefer this image among candidates. We use the official pretrained HPSv2.1 checkpoint and feed it our generated images and prompts. The predicted score is used as a reward that reflects human aesthetic and semantic preferences.

PickScore [27]. PickScore is another human-preference model built on top of a CLIP backbone and trained on a large-scale dataset. For each image-prompt pair, PickScore outputs a scalar preference score that correlates with human judgments of overall quality.

GenEval [17]. GenEval is a compositional evaluation benchmark designed to test whether a generated image satisfies fine-grained constraints such as the presence, count, and color of objects described in the prompt. During training, we follow its official evaluation pipeline: for each prompt, the metadata specifies the required object categories, counts, or colors. We then apply the GenEval detectors to the generated image and check whether all constraints are satisfied. The GenEval reward is set to 1 if the image passes all checks and 0 otherwise, encouraging the policy to generate images that strictly follow the compositional instructions.

OCR [6]. To assess text rendering quality, we use an OCR-based reward. For prompts that require specific characters or strings to appear in the image, the metadata stores the target text. We run an off-the-shelf OCR recognizer on the generated image to extract all visible text and compute the fraction of target characters that are correctly recognized in the OCR output. This fraction is used as the OCR reward, which directly encourages the model to produce images with legible and accurate text. We use paddleocr as the reward model.

F.4 Critic Models

We explore several off-the-shelf vision-language models as the backbone of our critic. In all cases, the critic takes the generated image and its corresponding prompt as input and outputs a scalar score, which we interpret as the value of this image-prompt pair. Concretely, we consider three families of critics: (i) a CLIP-based critic, (ii) a BLIP-based critic, and (iii) a critic initialized from a pretrained reward model. Our ablations are mainly conducted on HPSv2.1, therefore we adopt the HPSv2.1-based critic as the default choice in our experiments.

CLIP Critic. For the CLIP critic, we use a pretrained CLIP model and keep both the image and text encoders frozen. Given a prompt and a generated image, we obtain the text embedding and image embedding from CLIP and compute their cosine similarity. This design leverages the strong text-image alignment capability of CLIP while keeping the critic architecture simple and stable.

BLIP [31] Critic. BLIP is a vision-language model originally designed for image captioning and vision-language understanding. Similar to the CLIP critic, we use the BLIP image encoder and text encoder to extract image and text embeddings for each image-prompt pair. We then compute the cosine similarity between these two embeddings and take it as the BLIP critic score. Compared to CLIP, BLIP provides a different inductive bias focused on captioning and language understanding, offering a complementary critic signal. In our experiments, we use blip-itm-base-coco to initialize the critic model.

Reward-model-initialized Critic. Finally, we investigate using a pretrained reward model as the initialization for our critic. In this setting, we start from the HPSv2.1 checkpoint, which is trained on large-scale human preference data. We use the output reward score directly as the critic value. During our RL training, this HPSv2.1-based critic can be further fine-tuned together with the policy, allowing the critic to stay aligned with human preference while adapting to the distribution induced by our policy.

F.5 Inference Guidance

We compare our method against two inference-time baselines that only use the frozen generator and a pretrained reward/critic model at test time: Best-of- N (BoN) and Sequential Monte Carlo (SMC). Both Baselines operate on top of the same diffusion sampler and use the same reward model or critic as our method to score candidate images.

Best-of- N (BoN). Best-of- N is a widely-used test-time selection baseline. For each input prompt, we independently draw N samples from the diffusion model using the standard sampling configuration described above. We then evaluate each generated image with the corresponding reward model (e.g., CLIP, HPSv2.1, or other task-specific reward) and obtain a scalar score. The final output for this prompt is chosen as the image with the highest reward among the N candidates.

Sequential Monte Carlo (SMC). Sequential Monte Carlo [10] provides a more structured test-time procedure that uses a population of samples (particles) and iteratively refines them guided by the reward/critic. For each prompt p , we maintain K particles $\{x_t^{(i)}\}_{i=1}^K$ along the diffusion time steps $t = 0, \dots, T$. At every step, SMC performs propagation, reweighting, and resampling so that computation is focused on high-reward regions of the sample space.

We initialize particles from the standard Gaussian prior with uniform weights:

$$x_T^{(i)} \sim \mathcal{N}(0, I), \quad w_T^{(i)} = \frac{1}{K}, \quad i = 1, \dots, K. \quad (9)$$

Then, for each diffusion step $t = T - 1, \dots, 0$, we proceed as follows:

Propagation. Each particle is propagated by one step of the diffusion sampler \mathcal{T}_t (e.g., DDIM / Euler update) conditioned on the prompt p :

$$\tilde{x}_{t-1}^{(i)} = \mathcal{T}_t(x_t^{(i)}, \epsilon_t^{(i)}), \quad (10)$$

where $\epsilon_t^{(i)}$ is the sampler noise and $\tilde{x}_{t-1}^{(i)}$ denotes the propagated (pre-resampling) particle.

Reweighting. We evaluate the critic (or reward model) f_ψ on each propagated particle and convert the scalar score into an unnormalized weight, for example, using an exponential mapping with temperature τ :

$$\tilde{w}_{t-1}^{(i)} = \exp\left(\frac{1}{\tau} f_\psi(\tilde{x}_{t-1}^{(i)}, p)\right), \quad (11)$$

$$w_{t-1}^{(i)} = \frac{\tilde{w}_{t-1}^{(i)}}{\sum_{j=1}^K \tilde{w}_{t-1}^{(j)}}. \quad (12)$$

The normalized weights $\{w_t^{(i)}\}_{i=1}^K$ concentrate probability mass on high-critic-score particles.

Resampling. Finally, we resample particles according to the normalized weights:

$$a_{t-1}^{(i)} \sim \text{Categorical}(w_{t-1}^{(1:K)}), \quad (13)$$

$$x_{t-1}^{(i)} = \tilde{x}_{t-1}^{(a_{t-1}^{(i)})}, \quad (14)$$

which duplicates high-weight particles and discards low-weight ones, yielding a new equally weighted set $\{x_t^{(i)}\}_{i=1}^K$ for the next step.

After the final diffusion step, we obtain a set of particles $\{x_0^{(i)}, w_0^{(i)}\}_{i=1}^K$. We use the critic to select the final output as the image with the highest score:

$$i^* = \arg \max_i f_\psi(x_0^{(i)}), \quad (15)$$

$$\hat{x} = x_0^{(i^*)}. \quad (16)$$

G Visual Results

Additional Results. We present additional qualitative examples generated by our aligned models in Fig. 11.



Figure 11: Additional visual results generated by our aligned models. All images are produced without classifier-free guidance (CFG).